Supplemental Information

Off-tumor targets compromise antiangiogenic drug sensitivity by inducing kidney erythropoietin production

Masaki Nakamura[1], Yin Zhang[1,2], Yunlong Yang[1], Ceylan Sonmez[1], Wenyi Zheng[1], Guichun Huang[1], Takahiro Seki[1], Hideki Iwamoto[1], Bo Ding[3], Linlin Yin[3], Theodoros Foukakis[4], Thomas Hatschek[4], Xuri Li[5], Kayoko Hosaka[1], Jiaping Li[6]*, Guohua Yu[7]*, Xinsheng Wang[2]*, Yizhi Liu[5]* and Yihai Cao[1,2,5]*

[1]Department of Microbiology, Tumor and Cell Biology, Karolinska Institute, 171 77 Stockholm, Sweden

[2]Central Research Laboratory, The Affiliated Hospital of Qingdao University, Qingdao, 266071, China

[3]Department of Hematology and Oncology, The Fourth Hospital of Jinan, Jinan, Shandong 250031, China

[4]Department of Oncology-Pathology, Karolinska Institutet, Karolinska University Hospital, 171 77 Stockholm, Sweden

[5]State Key Laboratory of Ophthalmology, Zhongshan Ophthalmic Center, Sun Yat-Sen University, Guangzhou 510060, China

[6]Department of Interventional Oncology, The First Affiliated Hospital; Zhongshan School of Medicine, Sun Yat-sen University, Guangzhou, 510080, P. R. China

[7]Wei Fang People's Hospital, Yu He Road 151, Kui Wen District, Weifang, Shandong, China

Key words: Tumor, angiogenesis, erythropoietin, hematopoiesis, drug resistance

*Corresponding authors

Supplemental Table 1. Blood counts of RBC, HGB, and HCT[1]

	Group	RBC (1×10^{12}/L)	HGB(g/L)	HCT(%)
Tumor-bearing mice	Non-treated healthy mice	8.67 ± 0.17	124.43 ± 2.95	37.74 ± 1.17
	NIIgG[2]	6.44 ± 0.32	104 ± 5.51	35.63 ± 1.84
	Anti-VEGF	6.80 ± 0.30	109 ± 6.11	37.37 ± 1.22
	NIIgG + sEPoR	6.50 ± 0.17	104 ± 3.02	35.10 ± 0.81
	Anti-VEGF + sEPoR	6.68 ± 0.54	106.50 ± 3.50	35.95 ± 2.95

[1] RBC = red blood cell; HGB = hemoglobin; HCT = hematocrit.

[2] NIIgG = non-immune IgG

Supplementary table 2. Patients' clinical and demographic characteristics

Patient Number	Gender	Age	Diagnosis	Stage	Metastatic Site	RBC[1] ($\times 10^{12}$)	Hb[2] (g/L)	HCT[3] (%)	Treatment
1	Male	51	Rectal Cancer	IV	Lung	3.91	119	36.0	FOLFOX[4]
2	Male	40	Rectal Cancer	IV	Liver, adrenal gland, bone	4.39	116	35.5	FOLFOX
3	Male	64	Colon Cancer	IV	Lung	4.52	137	41.3	FOLFOX
4	Male	31	Colon Cancer	IIIA(pT2N1bM0)	-	4.83	158	44.5	FOLFOX
5	Male	58	Rectal Cancer	IIIB(pT3N2aM0)	-	4.19	126	37.8	FOLFOX
6	Male	42	Colon Cancer	IV	Liver	4.98	116	37.8	FOLFOX
7	Male	54	Colon Cancer	IV	Peritoneal wall	4.32	137	39.9	FOLFOX
8	Male	64	Rectal Cancer	IV	Liver	4.98	145	43.7	FOLFOX
9	Male	54	Colon Cancer	IV	Liver, mesenteric lymph nodes	4.25	128	37.4	FOLFOX
10	Male	62	Colon cancer	IV	Peritoneal wall	3.95	128	38.7	XELOX[5]
11	Female	53	Colon cancer	IV	Liver	3.46	120	35.4	XELOX
12	Female	44	Colon cancer	IV	Peritoneal wall	3.85	120	36	FOLFIRI[6]
13	Male	72	Rectal cancer	IV	Liver, lung	4.46	147	43	XELOX

14	Male	65	Rectal cancer	IV	Liver, lung	4.52	129	37.7	FOLFOX
15	Male	49	Colon cancer	IV	Lung	4.63	130	40.4	FOLFOX
16	Female	47	Colon cancer	IV	Peritoneal wall	4.35	91	31	FOLFOX
17	Female	80	Rectal cancer	IV	Liver, mesenteric lymph nodes	4.07	122	34.5	FOLFOX
18	Male	53	Rectal cancer	IV	Peritoneal wall	3.42	99	30.3	XELOX
19	Male	57	Colon cancer	IV	Peritoneal wall	3.95	72	25.3	FOLFIRI
20	Male	75	Colon cancer	IV	Liver, mesenteric lymph nodes	4.11	129	38.1	FOLFOX
21	Male	46	Rectal cancer	IV	Liver	4.33	124	0.377	FOLFOX
22	Female	75	Rectal cancer	IV	Peritoneal wall	4.93	135	41.2	FOLFOX
23	Male	30	Colon cancer	IV	Liver	4.68	145	41.9	XELOX
24	Female	53	Colon cancer	IV	Peritoneal wall	3.83	132	39.1	XELOX
25	Male	35	Colon cancer	IV	Lung	4.09	131	37.6	FOLFOX
26	Male	52	Colon cancer	IV	Peritoneal wall	3.42	113	34.9	FOLFOX
27	Male	61	Rectal cancer	IV	Liver	4.78	147	43.8	FOLFOX

28	Male	45	Colon cancer	IV	Peritoneal wall	4.52	124	37.9	XELOX
29	Male	33	Colon cancer	IV	Lung	4.13	123	37.1	FOLFIRI
30	Female	53	Colon cancer	IV	Liver, lung	3.6	126	35.8	XELOX
31	Female	53	Colon cancer	IV	Liver	3.43	114	33.5	XELOX
32	Female	53	Colon cancer	IV	Lung	3.64	120	35.8	XELOX
33	Female	53	Colon cancer	IV	Peritoneal wall	3.88	127	36.6	XELOX
34	Male	60	Colon cancer	IV	Peritoneal wall	3.90	128	38.5	FOLFOX
35	Male	47	Colon cancer	IV	Peritoneal wall	4.25	138	41.1	Bevacizumab+FOLFOX
36	Male	61	Colon cancer	IV	Liver	4.29	120	36.7	Bevacizumab+FOLFOX
37	Male	57	Colon cancer	IV	Liver, mesenteric lymph nodes	4.41	141	41.3	Bevacizumab+FOLFOX
38	Female	46	Rectal cancer	IV	Liver	4.67	124	38.2	Bevacizumab+FOLFOX
39	Male	52	Rectal cancer	IV	Lung	4.77	148	43.6	Bevacizumab+FOLFOX
40	Male	76	Colon cancer	IV	Liver, lung	4.22	126	37.8	Bevacizumab+FOLFOX
41	Female	47	Colon cancer	IV	Liver	3.78	128	35.8	Bevacizumab+FOLFOX

42	Male	51	Rectal cancer	IV	Lung	4.16	124	37.8	Bevacizumab+FOLFOX
43	Male	68	Colon cancer	IV	Lung	4.4	128	40.8	Bevacizumab+FOLFOX
44	Male	74	rectal cancer	IV	Liver	4.68	121	38	Bevacizumab+FOLFIRI
45	Male	62	rectal cancer	IV	Liver, mesenteric lymph nodes	5.24	156	47.2	Bevacizumab+FOLFIRI
46	Male	57	Colon cancer	IV	Liver, lung	4.61	108	35.5	Bevacizumab+XELOX
47	Male	41	Colon cancer	IV	Peritoneal wall	4.57	138	41.6	Bevacizumab+FOLFOX
48	Male	67	Colon cancer	IV	Liver, Peritoneal wall	4.65	140	42.8	Bevacizumab+FOLFOX
49	Male	75	Colon cancer	IV	Liver	4.29	141	41.5	Bevacizumab+FOLFOX
50	Female	68	Colon cancer	IV	Liver	3.75	125	36.9	Bevacizumab+FOLFOX
51	Male	67	Colon cancer	IV	Peritoneal wall	4.13	137	39.3	Bevacizumab+ XELOX
52	Female	63	Rectal cancer	IV	Liver	3.75	121	36.8	Bevacizumab+ XELOX
53	Female	53	Rectal cancer	IV	Liver, peritoneal wall	3.65	117	33.4	Bevacizumab+FOLFOX
54	Male	47	Colon cancer	IV	Peritoneal wall	4.64	142	43.4	Bevacizumab+FOLFOX
55	Male	61	Colon cancer	IV	Liver	4.69	129	39.7	Bevacizumab+FOLFOX

56	Male	57	Colon cancer	IV	Liver, mesenteric lymph nodes	4.73	149	43.8	Bevacizumab+FOLFOX
57	Female	46	Rectal cancer	IV	Liver	4.73	121	38.5	Bevacizumab+FOLFOX
58	Male	52	Rectal cancer	IV	Lung	4.74	146	42.7	Bevacizumab+FOLFOX
59	Male	76	Colon cancer	IV	Liver, lung	4.49	130	39.4	Bevacizumab+FOLFOX
60	Female	47	Colon cancer	IV	Liver	4	132	38	Bevacizumab+FOLFOX
61	Male	51	Rectal cancer	IV	Lung	4.07	123	37	Bevacizumab+FOLFOX
62	Male	47	Colon cancer	IV	Peritoneal wall	4.34	131	40.1	Bevacizumab+FOLFOX
63	Male	61	Colon cancer	IV	Liver	4.62	125	38.4	Bevacizumab+FOLFOX
64	Male	57	Colon cancer	IV	Liver, mesentericlymph nodes	4.46	144	41.7	Bevacizumab+FOLFOX
65	Female	46	Rectal cancer	IV	Liver	4.9	118	38.4	Bevacizumab+FOLFOX
66	Male	52	Rectal cancer	IV	Lung	4.9	148	44.2	Bevacizumab+FOLFOX

[1] RBC = red blood cell

[2] Hb = hemoglobin

[3] HCT = hematocrit

[4] FOLFOX = folinic acid, fluorouracil, and oxaliplatin

[5] XELOX = capecitabine and oxaliplatin

[6] FOLFIRI = folinic acid, fluorouracil, and irinotecan

Supplemental Table 3. Baseline characteristics and outcome of the 61 patients of the PROMIX trial included in the analysis

Characteristic	Value
Age - years	
Median	49.7
Range	33.2-69.2
Menopausal status - no.	
Premenopausal	40
Postmenopausal ≤5 years	7
Postmenopausal >5 years	14
Baseline tumor size - mm	
Median	60
Range	20-180
Baseline axillary nodal status	
Negative	17
Positive (verified)	36
Unknown / uncertain	8
Baseline hormone receptor status - no.	
ER and/or PgR positive	42
ER-and PgR-negative	19
Baseline cell proliferation value (Ki67 % positive cells)	
≤20%	20
>20%	36
Missing	5
Pathological complete response (pCR) at surgery	
Yes	10
No	51
Disease status*	
Free of relapse	42
Relapse or death	19
Vital status*	
Alive	47
Deceased	14

*after a median follow up of 63.6 months

Supplemental Figures

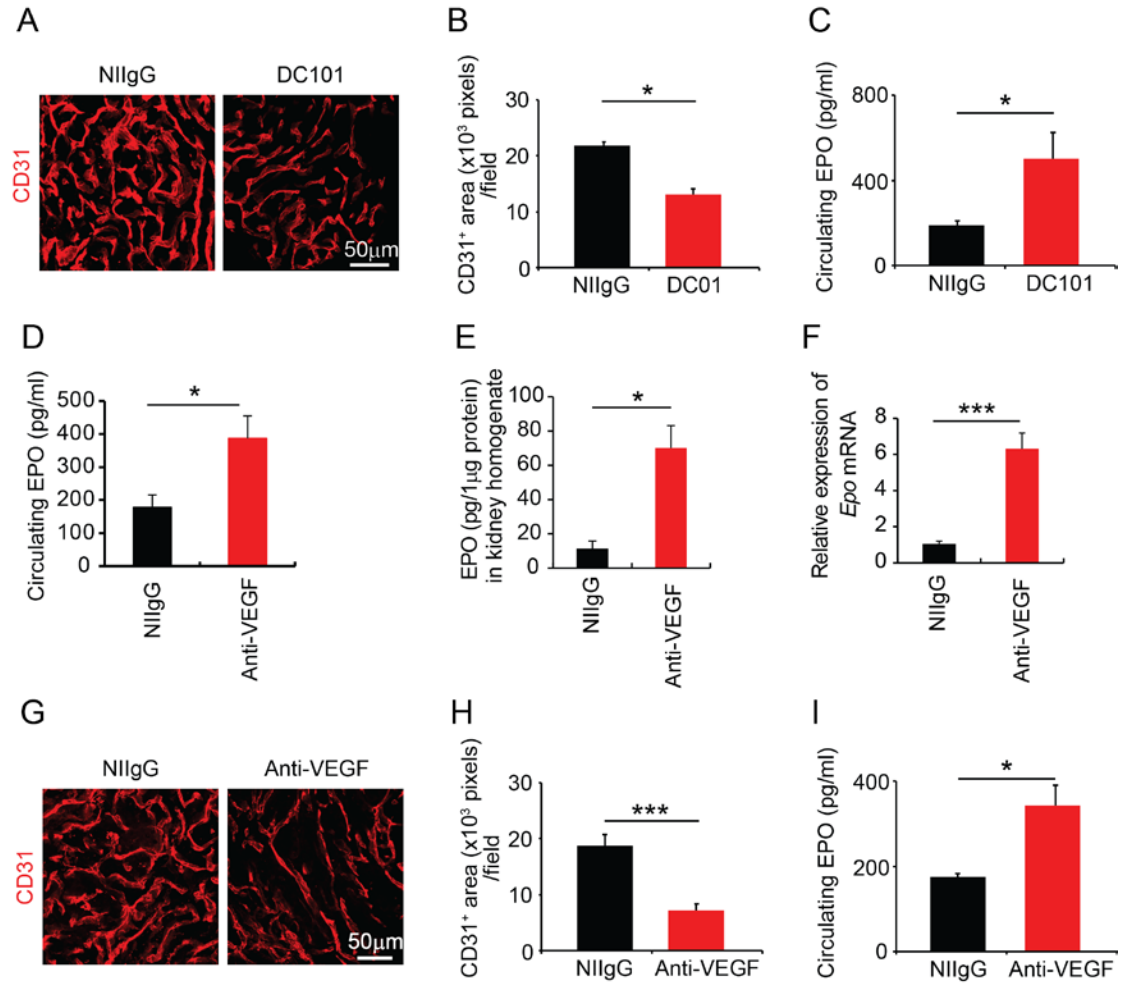

Supplemental Figure 1. Anti-VEGF induces kidney EPO production in tumor-free animals

(A) Kidney cortex $CD31^+$ microvessels in tumor free mice treated with NIIgG and DC101.

(B) Quantification for $CD31^+$ microvessels in tumor free mice kidney cortex (n = 6 samples per group). *$p < 0.05$.

(C) ELISA analysis of plasma EPO protein levels NIIgG- and DC101-treated tumor-free animals (n = 6 samples per group). *$p < 0.05$.

(D) ELISA analysis of plasma EPO protein levels of NIIgG- and anti-VEGF-treated tumor-free animals (n = 6 samples per group). *$p < 0.05$.

(E-F) ELISA analysis of EPO protein levels and qPCR analysis of *Epo* mRNA levels of the NIIgG- and anti-VEGF-treated kidney cortex (n = 6 samples per group). *$p < 0.05$; ***$p < 0.001$. Data are means ± s.e.m.

(G) Kidney cortex $CD31^+$ microvessels in 12-month old tumor free mice treated with NIIgG and anti-VEGF.

(H) Quantification for $CD31^+$ microvessels in old mice kidney cortex (n = 6 samples per group). ***$p < 0.001$.

(I) ELISA analysis of plasma EPO protein levels of NIIgG- and anti-VEGF-treated old mice (n = 6 samples per group). *$p < 0.05$.

A

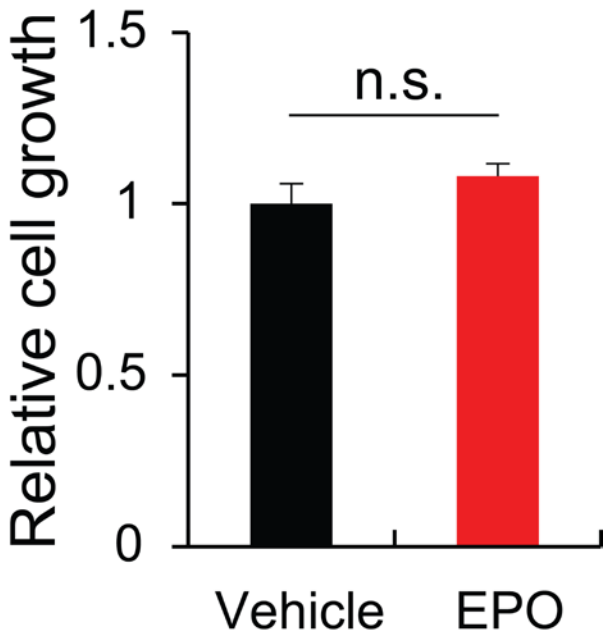

Supplemental Figure 2. EPO effect on LLC tumor cell proliferation

(A) Proliferation of vehicle- and rhEPO-treated LLC tumor cells was analyzed using a MTT assay (n = 6 samples per group). n.s. = not significant. Data are means ± s.e.m.

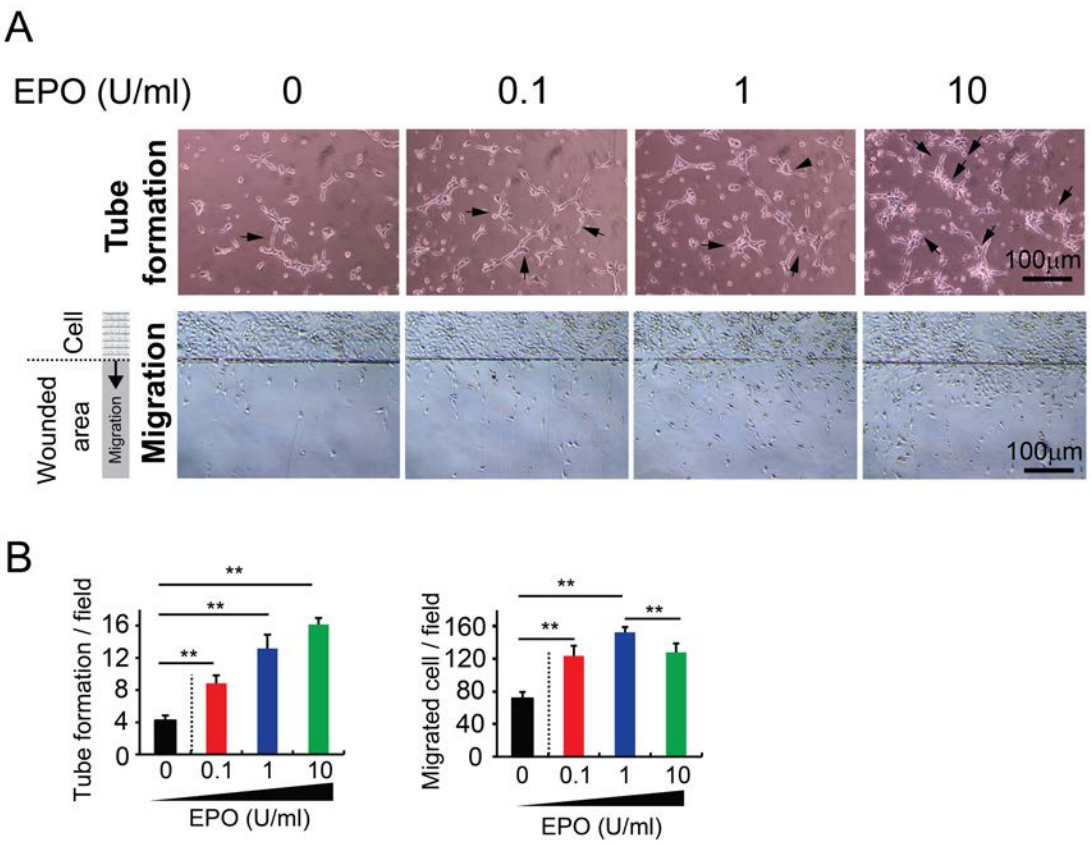

Supplemental Figure 3. EPO-EpoR-triggered endothelial cell signaling and functions

(A&B) Representative images of endothelial cell tube formation and migrating cells in the presence or absence of various concentrations of EPO protein. Quantifications of endothelial cell tube formation and migration (n = 8 random fields per group; quadruplicate per group). Scale bars = 100 μm. $^{**}p < 0.01$. Data are means ± s.e.m.

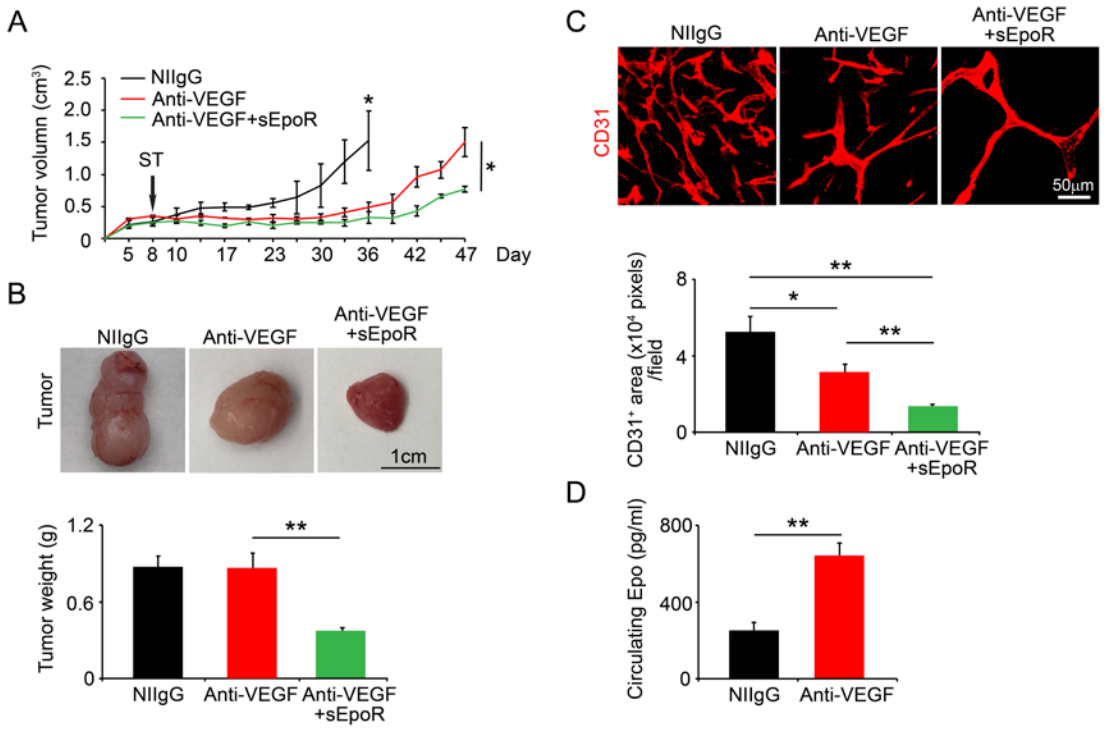

Supplemental Figure 4. Enhanced antitumor and antiangiogenic effects of anti-VEGF plus soluble Epo combination therapy in a human glioma model

(A) Tumor growth rates (n = 4 animals per group).

(B) Tumor mass and Tumor weight (n = 4 animals per group).

(C) Immunohistochemical analyses of $CD31^+$ microvessels vessels. Scale bar = 50 μm. Quantifications of $CD31^+$ vessel density and dextran blood perfusion (n = 6 samples per group).

(D) Circulating Epo levels after NIIgG and Anti-VEGF treatment (n = 3 animals per group).

*$p < 0.05$; **$p < 0.01$. Data are means ± s.e.m.

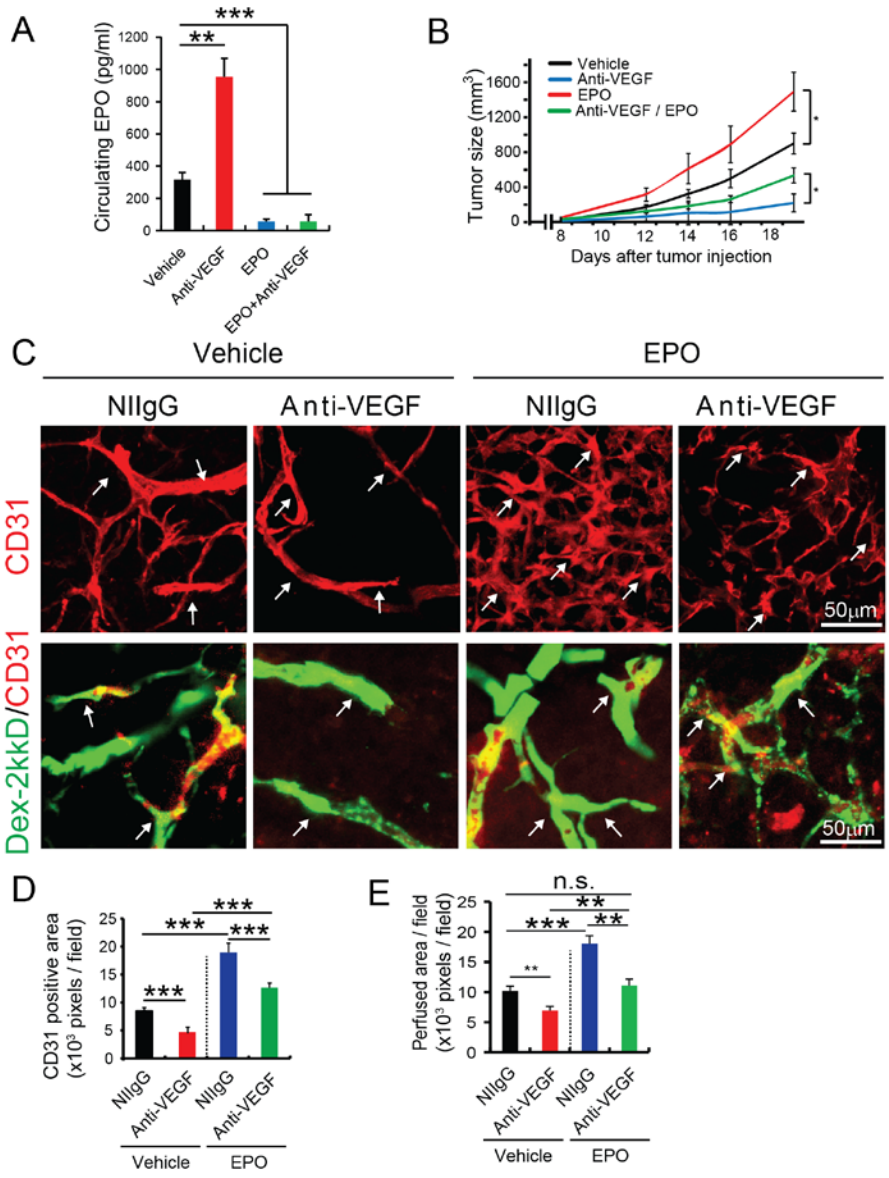

Supplemental Figure 5. Extragenous EPO induces anti-VEGF resistance in a fibrosarcoma model

(A) Quantitative measurement of circulating EPO protein by ELISA (n = 4-5 samples per group).

(B) Tumor growth rates of NIIgG-, anti-VEGF-, rhEPO-, and anti-VEGF plus rhEPO combination-treated T241 tumor-bearing mice (n = 6 animals per group). *$p < 0.05$. n.s. = not significant.

(C) Immunohistochemical analyses of $CD31^+$ microvessels and vascular perfusion of 2000 kD dextran of NIIgG-, anti-VEGF-, rhEPO-, and anti-VEGF plus

rhEPO combination-treated T241 tumors. Arrows in upper panels of **B** point to $CD31^+$ blood vessels and in lower panels indicate perfused $dextran^+$ signals. Scale bar = 50 μm.

(D & E) Quantifications of $CD31^+$ vessel density and dextran blood perfusion (n = 10 samples per group). $^{**}p < 0.01$; $^{***}p < 0.001$. n.s. = not significant. Data are means ± s.e.m.

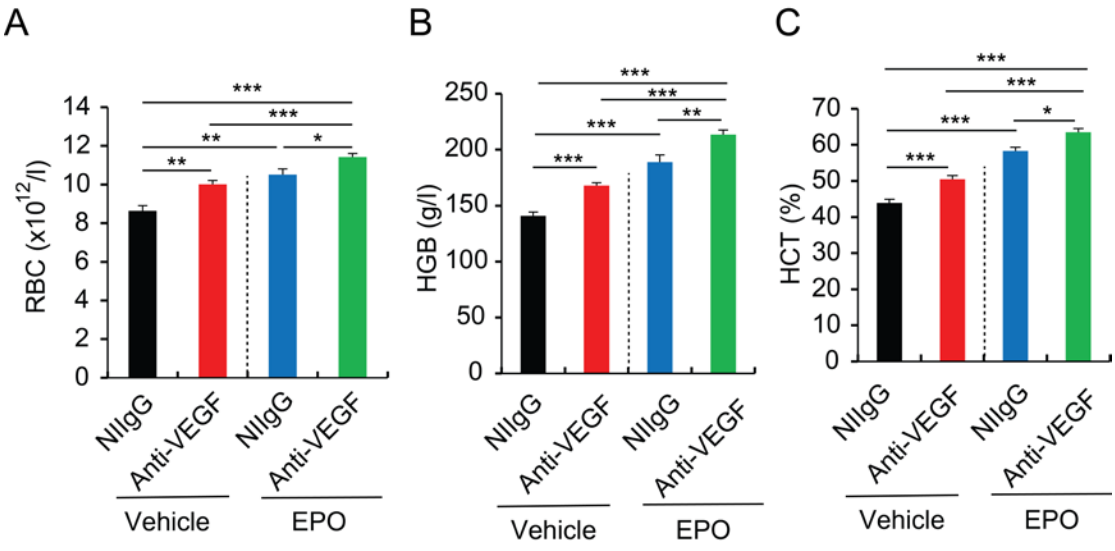

Supplemental Figure 6. Exogenous EPO effect on hematocrit in T241 tumor-bearing mice

(A-C) Analyses of red blood cells, haemoglobin levels, and haematocrits of NIIgG-, anti-VEGF-, rhEPO-, and anti-VEGF plus rhEPO combination-treated T241 tumor-bearing mice (n = 6 animals per group). $^{*}p < 0.05$; $^{**}p < 0.01$; $^{***}p < 0.001$. Data are means ± s.e.m.

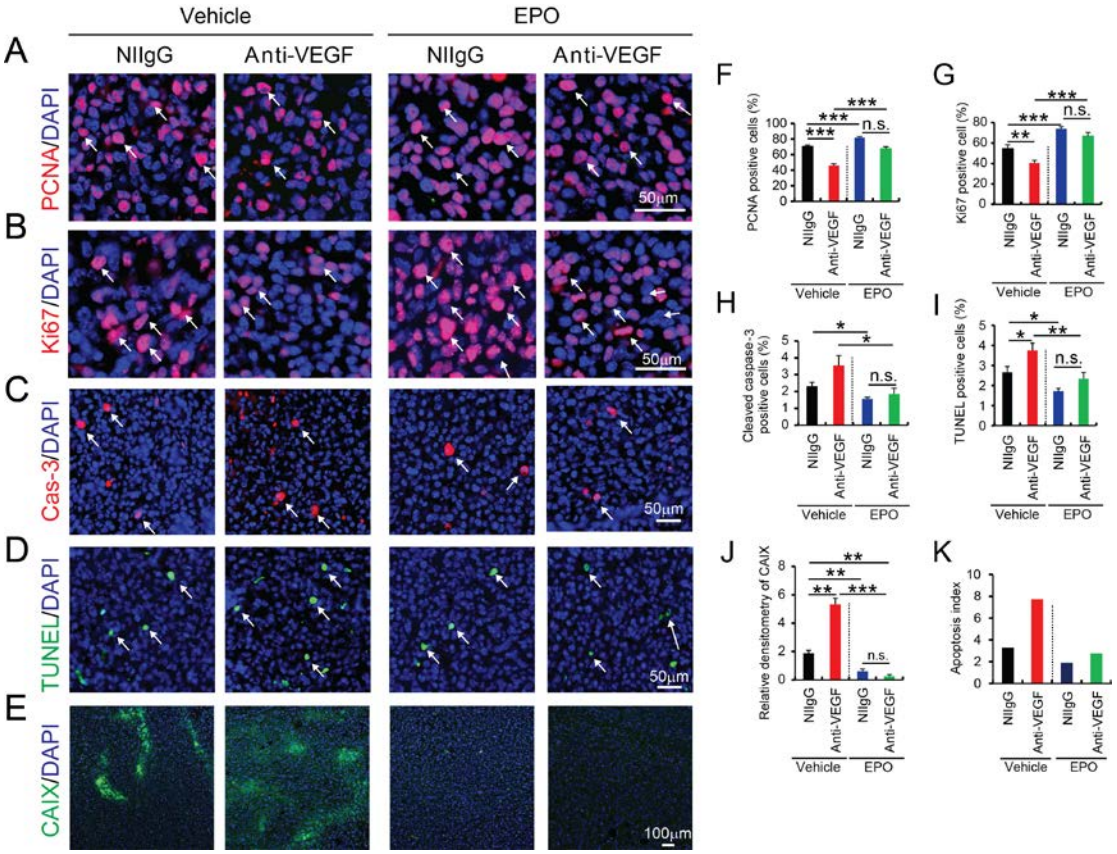

Supplemental Figure 7. EPO inhibits anti-VEGF-induced tumor cell proliferation, apoptosis, and hypoxia in a fibrosarcoma model

(A-E) Immunohistochemical analyses of $PCNA^+$ proliferating tumor cells, $Ki67^+$ proliferating tumor cells, cleaved $caspase\text{-}3^+$ apoptotic tumor cells, $TUNEL^+$ apoptotic tumor cells, and tumor hypoxia of NIIgG-, anti-VEGF-, rhEPO-, and anti-VEGF plus rhEPO combination-treated T241 tumors. Arrows in the first row panels indicate $PCNA^+$ proliferating tumor cells, in the second row panels indicate $Ki67^+$ proliferating tumor cells, in the third row panels indicate cleaved $caspase\text{-}3^+$ apoptotic tumor cells, and in the fourth row panels indicate $TUNEL^+$ apoptotic tumor cells. Scale bar = 50 μm. CAIX positive hypoxic signals are indicated with green signals in the fifth row panels. Scale bar = 100 μm. DAPI in blue was used for counter-staining of cell nuclei.

(F-K) Quantification of PCNA$^+$ proliferating tumor cells, Ki67$^+$ proliferating tumor cells, cleaved caspase-3$^+$ apoptotic tumor cells, TUNEL$^+$ apoptotic tumor cells, CAIX positive hypoxic signals, and apoptosis index (n = 10 random fields per group; 6 animals per group). *p < 0.05; **p < 0.01; ***p < 0.001; n.s. = not significant. Data are means ± s.e.m.

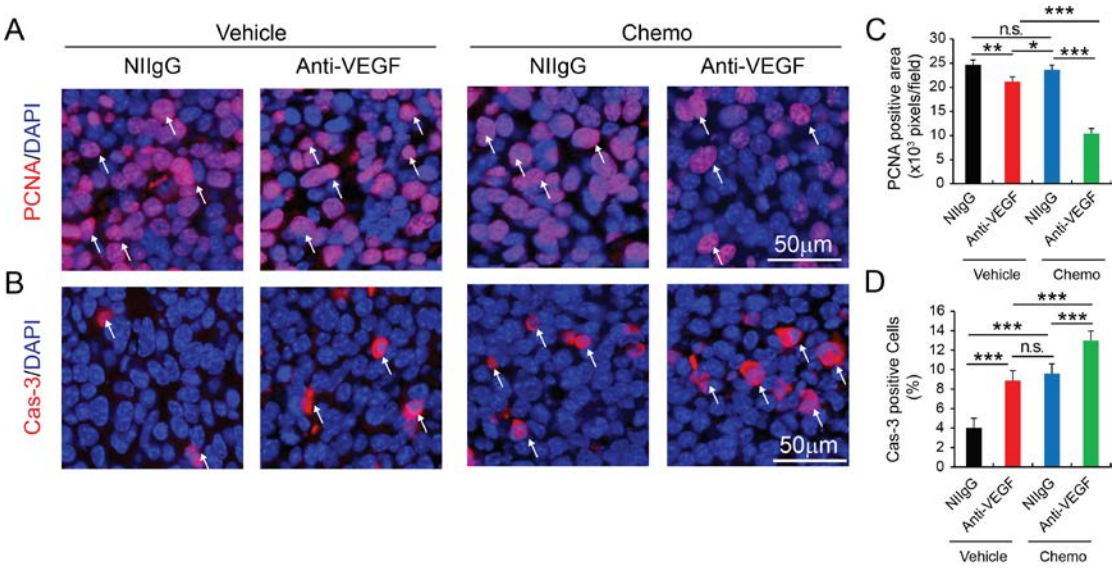

Supplemental Figure 8. Chemotherapy in combination of anti-VEGF therapy suppressed proliferation and induced apoptosis of tumor cells.

(A & B) Immunohistochemical analyses of PCNA$^+$ proliferating tumor cells, and cleaved caspase-3$^+$ apoptotic tumor cells of various monotherapy and combination therapy-treated LLC tumors. Arrows in the upper row panels indicate PCNA$^+$ proliferating tumor cells, and in the lower row panels indicate cleaved caspase-3$^+$ apoptotic tumor cells. Scale bar = 50 μm.

(C & D) Quantification of PCNA$^+$ proliferating tumor cells, and cleaved caspase-3$^+$ apoptotic tumor cells (n = 10 random fields per group; 6 animals per group). *p < 0.05; **p < 0.01; ***p < 0.001; n.s. = not significant. Data are means ± s.e.m

Supplemental Materials and Methods

Animals

Male 6- to 8-week-old C57Bl/6 mice were bred, acclimated and caged in groups of ten or fewer mice in the animal facility at the Department of Microbiology, Tumor and Cell Biology, Karolinska Institutet. Mice were anesthetized by injection of a 1:1:2 mixture of hypnorm (Veta-Pharma), dormicum (Roche) and distilled water before all surgical procedures and killed by a lethal dose of CO_2, which was followed by cervical dislocation. EpoR(-/-)::HG1-EpoR mice in C57Bl/6 background were purchased from the Experimental Animal Division, RIKEN BioResource Center (Tsukuba, Japan). *Epor* cDNA was fused to a genomic fragment containing Gata1-Hrd and the transgene constructs were injected into fertilized eggs derived from BDF1 parents and 6 independent lines of transgenic mice were obtained. Two lines of mice were crossed with EpoR+/- mice to create the mutant mice EpoR+/-::HG1-EpoR as previously described (1). All mouse studies were approved by the Animal Ethics Committee of Northern Stockholm.

Cell culture

Lewis Lung Carcinoma (LLC) , U87 and T241 fibrosarma cell lines (2, 3) were cultured in DMEM (HyClone; cat. no. SH30243.01) supplemented with 10% heat-inactivated FBS (HyClone; cat. no. SH30160.03), 100 U/ml penicillin, and 100 µg/ml streptomycin (HyClone; cat. no. SV30010). The UT-7/EPO cell line was kindly provided by Dr. Norio Komatsu at the Juntendo University, Tokyo, Japan. Cells were cultured in 10%

FBS-IMDM (GE healthcare; cat. no. SH30228.01) containing 1 U/ml recombinant human erythropoietin (rhEPO; Shenyang Sunshine Pharmaceutical; cat. no. S2001001).

Generation of sEpoR-Fc fusion protein

A cDNA fragment corresponding to the mouse soluble Epo receptor (4) was kindly provided by Dr. Masaya Nagao at the Kyoto University, Japan. This cDNA was modified and amplified by PCR using a pair of primers: forward primer: 5'-gggtcgacgcaccttcacccagcctcc-3'; and reverse primer: 5'-gggtcgacgggagtttgcctggtgtttg-3'. This modified fragment was subsequently cloned into a pME18S expression vector that was kindly provided by Dr. Hisashi Arase at the Osaka University, Japan. pME18S-IgG Fc vector or pME18S mouse sEpoR-IgG Fc plasmid DNA were transiently transfected into 293T cells in DMEM supplemented with ultra-low IgG FBS (Thermo Fisher Scientifc; cat. no. 16250086) for 2 days. Transfected cell supernatants were collected and Ig fusion proteins were purified using a protein A-sepharose affinity column (GE healthcare Life Sciences; cat. no. 17-5280-01).

Immunohistochemistry

Cryostat tissue sections in 8 μm thickness and PFA-fixed paraffin embedded tissue samples were incubated with specific antibodies against Ki67, PCNA, rabbit anti-mouse cleaved caspase-3 (Asp175) antibody (Cell Signaling; catalog no. 9661), CAIX, EpoR (proteintech, 55308-1-AP), or EPO, using our previously described immunohistochemical procedures (5, 6). An Alexa-555–conjugated goat anti-rat antibody (Life Technologies); an Alexa-555–conjugated goat anti-rabbit antibody (Life Technologies); an Alexa-488–conjugated donkey anti-rabbit antibody (Life Technologies), and a Cy5-conjugated goat anti-rat antibody (ChemiCon) were used as

secondary antibodies. For DAB staining, a horse raddish peroxidase (HRP) conjugated anti-rabbit antibody diluted with TBS in a ratio of 1:200 was used as a secondary antibody. After washing, slides were incubated with DAB (3,3'-diaminobenzidine tetrahydrochloride) (Sigma) and immediately washed under tap water after color development. Slides were counter-stained with hematoxylin. Stained slides were mounted with Pertex (Histolab; cat. no. 00801) and were observed under a light microscope.

Whole-mount staining

Tumor tissue whole-mount staining was performed as described previously (7). In brief, fresh tumor tissues were fixed at 4 °C overnight with 4% PFA, followed by washing with PBS. Tissues were cut into small and thin pieces by a scalpel, digested for 5 min with proteinase K in a 20 mM Tris buffer (pH 7.5), permeabilized with 100% methanol for 30 min, blocked in 3% milk in a 0.3% Triton X-100-PBS (Sigma-Aldrich; cat. no. X100) buffer, and incubated with anti-mouse CD31 (1:200; BD-Pharmingen, 553370) at 4 °C overnight. The primary antibody-stained tumor tissues were blocked further with 3% milk, followed by incubation for 2 h with Alexa Fluor 555-labelled goat anti-rat (1:400; Invitrogen, A21434) secondary antibody at room temperature. Tissues were washed at 4 °C overnight thoroughly with PBS before mounting in Vectashield mounting medium (Vector Laboratories; cat. no. H-1000), and were subsequently stored at −20 °C until further analysis. Consecutive scanning of seven layers of each tissue sample was assembled to constitute a 3D-image dataset using a software program (Nikon, EZ-C1) analysis. Each dataset was quantified from at least 10 different random fields of using an Adobe Photoshop CS software program.

FACS analysis

The single cell suspension was prepared by a 0.40 μm-filter. Cells were stained for 45 min on ice with a rabbit anti-mouse EpoR antibody (1:100; proteintech, 55308-1-AP). After rigorous washing with PBS, cells were incubated with an Alexa Fluor 555-labelled goat anti-rabbit antibody for 20 min on ice. Expression of EpoR were analysed using an FACS analyser (MoFlo XTD, Beckman Coulter).

Blood sample analysis

Fresh animal blood was intracardially collected and plasma was prepared using the anticoagulant EDTA, followed by centrifugation. Hematological parameters including hemoglobin, hematocrit, red blood cell count were determined by an automated hematology analyzer (Mindray).

ELISA

Fifty milligrams of fresh kidney or tumor tissue were homogenized in a 500 μl lysis buffer (Cat. No. C3228, Sigma) containing a cocktail of proteinase inhibitors (Cat. No. P8340, Sigma) using an electronic homogenizer. Tissue homogenates were centrifuged at 12000 rpm for 15 min and 50 μl of supernatant from each sample were analysed using an ELISA kit detecting mouse EPO (Cat. No. MEP00B, R&D Systems Inc.) according to the manufacturer´s instruction. Blood samples from mice or human were collected using EDTA and centrifuged at 2000g for 20min. Plasma samples were collected and 50 μl of samples were analysed using an ELISA kit detecting human EPO (Cat. No. ab119522, Abcam).

Blood Perfusion

Briefly, 1 mg of 2000-kD-lysinated LRD (D7139; Invitrogen) lysinated LRD (D1818; Invitrogen) in 100 ml ddH2O was intravenously injected into the tail vein of each mouse. At 5-min post-injection, mice were sacrificed by cervical dislocation and tumors were removed. Tumor tissues were fixed overnight with 4% PFA, followed by whole-mount immunostaining. A rat anti-mouse CD31 (1:200; AP183S; Invitrogen,) and a Cy5-labelled goat anti-rat IgG secondary antibody (1:200; AP183S; Invitrogen,) were used for vessel staining. Positive signals were detected by confocal Microscopy (Nikon C1 Confocal microscope; Nikon Corporation, Japan)

TUNEL staining

Apoptotic cells in tumor tissues were detected using an in situ cell-death detection kit (Roche; catalog no. 11684795910) according to the manufacturer's protocol. After staining, the mounted samples were examined with a fluorescent microscope, and at least 10 random areas were measured for each group using a Photoshop software program (Adobe).

In vitro endothelial cell tube formation assay and migration assay

Primary mouse endothelial cells were isolated from tumor-free C57Bl/6 mice and used for in vitro assay as described previously (8). Uptake of acetylated–LDL (Biomedical Tec.) was validated in these cells. Cells were cultured in 10 % FBS-DMEM and less than 10 passages were used throughout our experiments. For the capillary-like tube formation assay, 1.5×10^4 cells were incubated in growth factor-reduced Matrigel (BD

Biosciences) in DMEM medium containing 0, 0.1, 1, and 10 U ml^{-1} of rhEPO in 24-well plates for 8 h (quadruplicate per group). Images were photographed by light microscopy (Nikon). Vessel-like tube area and length of capillary tubes were quantitatively analyzed using Adobe Photoshop or NIH-element D1 (Nikon) programs. For migration assay, monolyer endothelial cells were seeded at 90% confluency 24-well plates. Monolayer cells were detached with a sterile blade and cultured in medium containing 0, 0.1, 1, and 10 U ml^{-1} of rhEPO. After 48 h, migrated cells in the scratched area were photographed by light microscopy and counted using a NIH–element D1 software program (n = 5-6 samples per group).

Detection of hypoxia

The hypoxia probe pimonidazole hydrochloride (Hypoxyprobe; cat. no. HP2-1000 kit) was i.p. injected at a dose of 60 mg kg^{-1}. Tissue sections were subjected to immunofluorescent staining for CD31 and pimonidazole after rehydration. Antigen retrieval was done with a retrieval buffer (Cat. No. H3300, Vector laboratories) by boiling for 10 min. Sections were blocked with 4% goat serum for 30 min, followed by incubation at 4 ºC overnight with an anti-CD31 primary antibody (Cat. No. AF3628, R&D; 1:200 dilution) or an anti-pimonidazole (Cat. No. HP2-1000Kit, Hypoxyprobe; 1:200 dilution). Sections were further stained with a secondary donkey anti-goat Alexa 555 antibody (Cat. No. A21432, Invitrogen). Images were captured under fluorescent microscopy (ECLIPSE 90i, NIS-Element D, Nikon).

Proliferation assay

LLC and T241 tumor cells (1 x 10^4) were seeded onto each well of a 96-well plate. Cell proliferation (n = 6 samples per group) was analyzed at 48 h using a MTT (5 mg/mL;

M5655; Sigma-Aldrich) method. Densitometry absorbance at 490 nm was measured by a spectrophotometer.

RT-PCR and qPCR

Total tissue RNAs were extracted using a 2-mercaptoethanol–supplemented (Sigma-Aldrich; cat. no. 3148) lysis buffer supplied in a RNA extraction kit (Thermo Scientific; catalog no. K0732). Absolute ethanol was added to tissue lysates before purification thorough a column according to the manufacturer's protocol. Total amount of RNA was measured and 1 μg RNA was used for cDNA synthesis by reverse transcription (Thermo Scientific; cat. no. K1632). qPCR was performed with a Power SYBR Green master mix (Life Technologies; cat. no. 4367659) reaction in a Step-One Plus machine according to the manufacturer's instructions (Applied Biosystems). Following primers were used to detect specific mRNA expression: *mEpo*-sense 5'-agaatggaggtggaagaacagg-3'; *mEpo*-anti-sense 5'-ctggtggctgggaggaatt-3'; *mHif1a*-sense 5'-gtcggacagcctcaccaaacag-3'; *mHif1a*-anti-sense 5'-taggtagtgagccaccagtgtcc-3'; *mHif2a*-sense 5'-aatgacagctgacaaggagaaaaa-3'; *mHif2a* anti-sense 5'-gagtgaagtcaaagatgctgtgtc-3'; *mEpor*-sense 5'-ggacacctacttggtattgg-3'; *mEpor*-anti-sense 5'-gacgttgtaggctggagt-3';, and *mActin*-sense 5'-aggcccagagcaagagagg-3'; *mActin*-anti-sense 5'-tacatggcggggtgttgaa-3'.

Supplemental References

1. Suzuki N, *et al.* (2002) Erythroid-specific expression of the erythropoietin receptor rescued its null mutant mice from lethality. *Blood* 100(7):2279-2288.
2. Cao R, *et al.* (2004) PDGF-BB induces intratumoral lymphangiogenesis and promotes lymphatic metastasis. *Cancer cell* 6(4):333-345.
3. Eriksson A, *et al.* (2002) Placenta growth factor-1 antagonizes VEGF-induced angiogenesis and tumor growth by the formation of functionally inactive PlGF-1/VEGF heterodimers. *Cancer cell* 1(1):99-108.
4. Nagao M, Masuda S, Abe S, Ueda M, & Sasaki R (1992) Production and ligand-binding characteristics of the soluble form of murine erythropoietin receptor. *Biochemical and biophysical research communications* 188(2):888-897.
5. Ji H, *et al.* (2014) TNFR1 mediates TNF-alpha-induced tumour lymphangiogenesis and metastasis by modulating VEGF-C-VEGFR3 signalling. *Nature communications* 5:4944.
6. Hosaka K, *et al.* (2013) Tumour PDGF-BB expression levels determine dual effects of anti-PDGF drugs on vascular remodelling and metastasis. *Nature communications* 4:2129.
7. Dong M, *et al.* (2013) Cold exposure promotes atherosclerotic plaque growth and instability via UCP1-dependent lipolysis. *Cell metabolism* 18(1):118-129.
8. Xue Y, *et al.* (2012) PDGF-BB modulates hematopoiesis and tumor angiogenesis by inducing erythropoietin production in stromal cells. *Nature medicine* 18(1):100-110.